International Journal of Power Electronics and Drive System (IJPEDS)
Vol. 4, No. 2, June 2014, pp. 173~191
ISSN: 2088-8694

Application of Backstepping to the Virtual Flux Direct Power Control of Five-Level Three-Phase Shunt Active Power Filter

Bouzidi Mansour[*,], Bouafia Saber[**], Bouzidi Ali[***], Benaissa Abdelkader[**], Barkat Said[****]**
* Department of Electronics and Communications, Faculty of New Technologies of Information and Communication University Kasdi Merbah, Ouargla, Algeria.
** Department of Electrical Engineering, Faculty of Engineering, University of Djilali Liabes, Sidi Bel Abbes, Algeria, Intelligent Control Electronic Power System laboratory (I.C.E.P.S)
*** Department of Electrical Engineering, Faculty of Technology, University of Hadj Lakhdar Batna
**** Department of Electrical Engineering, Faculty of Engineering, M'sila University, M'sila, Algeria.

Article Info

Article history:

Received Jan 11, 2014
Revised Mar 13, 2014
Accepted Mar 26, 2014

Keyword:

Five-level shunt active power filter
Direct power control
Virtual flux concept
Backstepping control
Multilevel space vector modulation

ABSTRACT

This paper proposes a virtual flux direct power control-space vector modulation combined with backstepping control for three-phase five-level neutral point clamped shunt active power filter. The main goal of the proposed active filtering system is to eliminate the unwanted harmonics and compensate fundamental reactive power drawn from the nonlinear loads. In this study, the voltage-balancing control of four split dc capacitors of the five-level active filter is achieved using five-level space vector modulation with balancing strategy based on the effective use of the redundant switching states of the inverter voltage vectors. The obtained results showed that, the proposed multilevel shunt active power filter with backstepping control can produce a sinusoidal supply current with low harmonic distortion and in phase with the line voltage.

Corresponding Author:

Bouzidi Mansour,
Department of Electronics and Communications,
Faculty of New Technologies of Information and Communication
University Kasdi Merbah, Ouargla, 30000, Algeria
Departement of Electrical Engineering,
Faculty of Engineering,
University of Djilali Liabes, Sidi Bel Abbes,
Sidi Bel Abbes 22000, Algeria
Email: bouzidi.m.28@gmail.com

1. INTRODUCTION

Nowadays the power electronic equipments are widely used in distribution networks which act as nonlinear loads. Many power quality disturbances such as harmonics pollution, unbalanced load currents, and reactive power problems are caused by the nonlinear loads; as a result poor power factor, weakening efficiency, over heating of motors and transformers, malfunction of sensitive devices etc.

To overcome the aforementioned problems passive filters can be used to compensate some of them. However, bulk passive components, series and parallel resonance and a fixed compensation characteristic are the main drawbacks of passive filters [1]. Therefore, to give an effective solution for harmonics concerns several active power filter (APF) topologies have been proposed. They aimed not only for current or voltage compensation but also for voltage dips, flicker and imbalance [2].

Among various active filter configurations, the shunt active power filters (SAPF) have a number of advantages [3]. Compared with the series and hybrid configurations, the SAPF do not need an additional coupling transformer and require much less protection and switchgear. They operate as three-phase controlled harmonic current sources and are not affected by harmonic distortions in supply voltages. In general, the ratings of shunt active power filters are based on the magnitudes of compensating current and the corresponding filter terminal voltage. For medium to high power applications the multilevel converters are the most attractive technology. Indeed, multilevel converters have shown some significant advantages over traditional two-level converters [4]-[7]. The main advantages of the multilevel converter are a smaller output voltage step, lower harmonic components, a better electromagnetic compatibility and lower switching losses [4]-[7]. In the recent time the use of multilevel inverters is prevailing in medium-voltage active power filters without using a coupling transformer [8]-[11].

Various control strategies have been proposed to control the SAPF, such as hysteresis band current control (HBCC) [12], voltage oriented control (VOC) [13]. Another interesting emerging control technique called direct power control (DPC) has been investigated [13], [14]. DPC is based on the instantaneous active and reactive power control loops. It is developed analogously with the well-known direct torque control (DTC) used for adjustable speed drives. In DPC, there are no internal current loops or modulator block because the converter switching states are selected via a switching table. Although DPC has many advantages, some disadvantages of this control technique are high ripple content in the system current, high ripple in the commanded active and reactive power, variable switching frequency, and requires a high switching frequency [15].

The DPC can be forced to operate at a constant frequency by using space vector modulation (SVM) to synthesize the space-vector voltage demanded by the switching table [15], [16]. Although classical DPC uses the fix number of vectors present in this table, more vectors can be arbitrarily generated by using SVM. In this way, the ripple in current can be reduced [15].

Recent developments have popularized the virtual flux (VF) concept, which assumes that both the grid and converter's line filter behave as an AC motor [17]. One of the main advantages of this approach is that it is less sensitive to line-voltage variations than other approaches. The virtual flux direct power control (VFDPC) is an adaptation of the DPC to a VF reference frame [17].

In this paper, a nonlinear control strategy based on the backstepping associated to VFDPC-SVM is applied to three-phase five-level shunt power active filter in the aim to improve its performances.

In the present study, it is shown via simulation results that the proposed backstepping controller has high performance both in the transient and in the steady state operations. The line currents are very close to sinusoidal waveforms, a good control of the DC-bus voltage is obtained, and unity power factor operation is achieved.

2. SHUNT APF CONFIGURATION

2.1. System Description

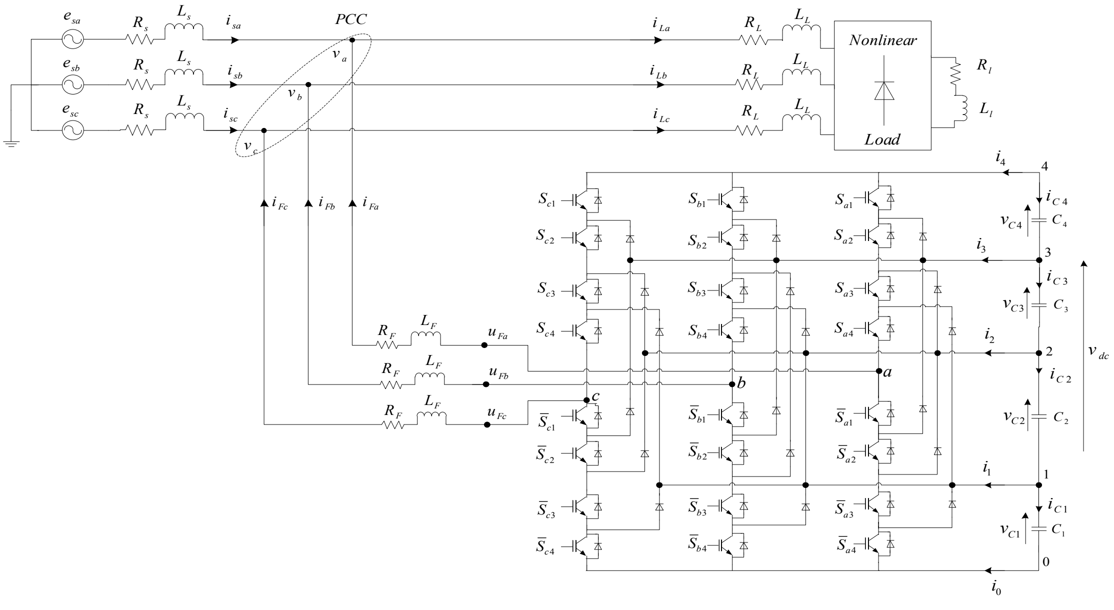

Figure 1. Five-level shunt active power filter configuration

The structure in Figure 1, describes the proposed SAPF based on a three-phase five-level VSC. The SAPF consists of three principal parts, the three-phase converter, four capacitors (C_1, C_2, C_3, and C_4) and the smoothing inductances L_F. The converter is used to charge and to discharge the capacitors to provide the required compensating current.

The capacitors are used to store energy and the inductances L_F are used to smooth and decrease the ripples of the harmonic currents injected by SAPF [9].

The main task of the SAPF is to reduce harmonic currents and to ensure reactive power compensation. Ideally, the SAPF needs to generate just enough reactive and harmonic current to compensate the nonlinear load harmonic in the line. The resulting total current drawn from the AC main is sinusoidal.

2.2. Modeling of the PWM five-level inverter

The topology of the three-phase five-level NPC inverter is shown also in Figure 1. Here, v_x and i_{Fx} , $x = a, b, c$, represent the point of common coupling (PCC) voltages and AC side currents, respectively. R_F is a line resistance that models the parasitic resistive effects of the inductor L_F. The capacitances of input capacitors are assume equal C_1=C_2=C_3=C_4=C. For a net dc-side voltage of v_{dc}, each capacitor voltage is ideally $v_{Cj} = v_{dc}/4$, $j = 1,..., 4$ and each generated phase voltage u_{Fx}, $x = a, b, c$, has five levels with respect to dc-side reference point 0. The switching states and the resultant phase voltages are listed in Table 1, where state conditions 1 and 0 indicate ON and OFF switch status, respectively.

Table 1. Switching states of a five-level inverter

Switching state	S_1	S_2	S_3	S_4	$\bar{S}_1$	$\bar{S}_2$	$\bar{S}_3$	$\bar{S}_4$	Phase voltage
4	1	1	1	1	0	0	0	0	v_{dc}
3	0	1	1	1	1	0	0	0	$3v_{dc}/4$
2	0	0	1	1	1	1	0	0	$v_{dc}/2$
1	0	0	0	1	1	1	1	0	$v_{dc}/4$
0	0	0	0	0	1	1	1	1	0

The switching functions of the five level inverter of Figure 1, are expressed as:

$$\begin{aligned} F_{x4} &= S_{x4}\ S_{x3}\ S_{x2}\ S_{x1} \\ F_{x3} &= S_{x4}\ S_{x3}\ S_{x2}\ \bar{S}_{x1} \\ F_{x2} &= S_{x4}\ S_{x3}\ \bar{S}_{x2}\ \bar{S}_{x1} \qquad x = a, b \text{ ou } c \\ F_{x1} &= S_{x4}\ \bar{S}_{x3}\ \bar{S}_{x2}\ \bar{S}_{x1} \\ F_{x0} &= \bar{S}_{x4}\ \bar{S}_{x3}\ \bar{S}_{x2}\ \bar{S}_{x1} \end{aligned} \tag{1}$$

Referring all of the voltages to the lower DC-link voltage level ("0" reference), each output voltage consists of contributions by a determinate number of consecutive capacitors:

$$u_{x0} = \sum_{j=0}^{4}\left(F_{xj}\sum_{i=0}^{j} v_{C_i}\right), \qquad x = a,\ b,\ c \tag{2}$$

When balanced distribution of the DC-link voltage among the capacitors is assumed:

$$u_{x0} = \frac{v_{dc}}{4}\sum_{j=0}^{4} jF_{xj}, \qquad x = a,\ b,\ c \tag{3}$$

The line to line voltage is given by:

$$\begin{bmatrix} u_{ab} \\ u_{bc} \\ u_{ca} \end{bmatrix} = \begin{bmatrix} u_{a0} - u_{b0} \\ u_{b0} - u_{c0} \\ u_{c0} - u_{a0} \end{bmatrix} \tag{4}$$

The expressions of instantaneous inverter phase output voltages are given by:

$$\begin{bmatrix} u_{Fa} \\ u_{Fb} \\ u_{Fc} \end{bmatrix} = \frac{1}{3}\begin{bmatrix} u_{ab} - u_{ca} \\ u_{bc} - u_{ab} \\ u_{ca} - u_{bc} \end{bmatrix} \tag{5}$$

2.3. Mathematical model of three-phase five levels SAPF

The mathematical equations which govern the behaviour of the ac-side of shunt active filter are:

$$\begin{aligned} \frac{di_{Fa}}{dt} &= \frac{1}{L_F}(u_{Fa} - v_a - R_F i_{Fa}) \\ \frac{di_{Fb}}{dt} &= \frac{1}{L_F}(u_{Fb} - v_b - R_F i_{Fb}) \\ \frac{di_{Fc}}{dt} &= \frac{1}{L_F}(u_{Fc} - v_c - R_F i_{Fc}) \end{aligned} \tag{6}$$

Where, $u_{Fi}, i = a,b,c$ represent voltages of the SAPF.

By transforming (6) in stationary frames, it follows that:

$$\begin{aligned} \frac{di_{F\alpha}}{dt} &= \frac{1}{L_F}(u_{F\alpha} - v_\alpha - R_F i_{F\alpha}) \\ \frac{di_{F\beta}}{dt} &= \frac{1}{L_F}(u_{F\beta} - v_\beta - R_F i_{F\beta}) \end{aligned} \tag{7}$$

Where, v_α and v_β are the PCC voltages in the stationary α-β coordinates. $i_{F\alpha}$ and $i_{F\beta}$ are *α-β* components of *AC* currents of SAPF. $u_{F\alpha}$ and $u_{F\beta}$ are *α-β* components of AC side voltages of SAPF.

The DC side of the filter can be expressed as:

$$\frac{dv_{dc}}{dt} = \frac{d}{dt}(v_{C1} + v_{C2} + v_{C3} + v_{C4}) \tag{8}$$

Equation (8) can also be written as:

$$\frac{dv_{dc}}{dt} = \frac{1}{C}(i_{C1} + i_{C2} + i_{C3} + i_{C4}) \tag{9}$$

Where i_{Cj} (j =1,2,3,4) is the current through capacitor C_j.

The equation of DC side (9) can be related to the AC side by the following power-balance relationship:

$$v_{C1}i_{C1} + v_{C2}i_{C2} + v_{C3}i_{C3} + v_{C4}i_{C4} = v_a i_{Fa} + v_b i_{Fb} + v_c i_{Fc} \tag{10}$$

If we assume that the capacitor voltages are balanced, the equation (9) becomes:

$$\frac{dv_{dc}}{dt} = \frac{1}{C_{eq} v_{dc}}(v_a i_{Fa} + v_b i_{Fb} + v_c i_{Fc}) \tag{11}$$

Where: $C_{eq} = C / 4$.

Equation (11) can be expressed as:

$$\frac{dv_{dc}}{dt} = \frac{p_F}{C_{eq}} \tag{12}$$

Where: p_F is the instantaneous active power of SAPF.

$$p_F = v_\alpha i_{F\alpha} + v_\beta i_{F\beta} \tag{13}$$

3. NONLINEAR VIRTUAL FLUX BASED DIRECT POWER CONTROL

The backstepping VFDPC-SVM control strategy main scheme is presented in Figure 2. The nonlinear load and SAPF currents are sensed using tow current sensors located in phases (a) and (b), and the estimated *PCC* virtual flux components $\psi_{PCC\alpha}$, $\psi_{PCC\beta}$ are used for the powers estimation (p_L, q_L and p_F, q_F) and backstepping power controller.

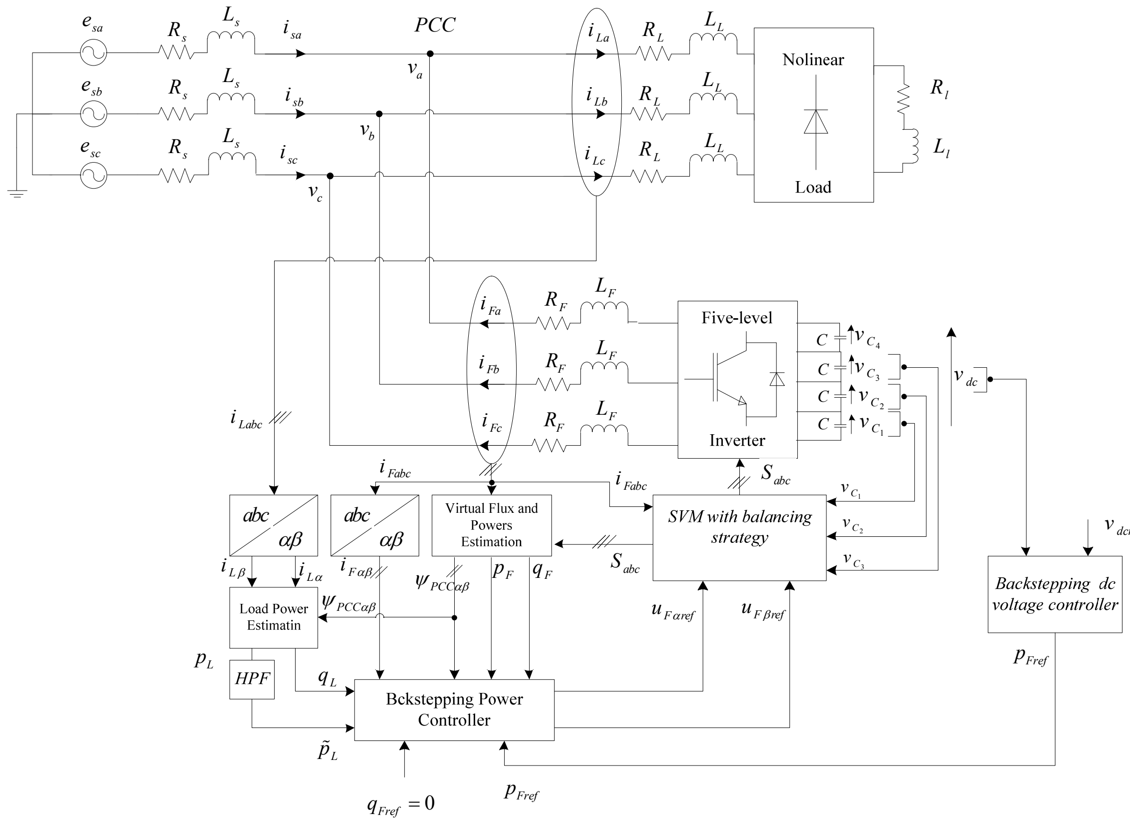

Figure 2. Backstepping VFDPC-SVM scheme of five-level SAPF

The active power p_L is delivered to the high pass filter (HPF) to obtain the alternate values, which finally are used as compensating component. The reactive power q_L can be delivered to the HPF or directly to the input of the backstepping power controller depending on compensation requirements (compensation of higher harmonics or compensation of higher harmonics and reactive power at the same time). The reference active power p_{Fref} (generated by the outer nonlinear DC voltage controller) and reactive power reference q_{Fref} (set to zero for unity power factor) values are compared with estimated instantaneous p_F and q_F values augmented by their corresponding alternate load powers p_L and q_L, respectively. The errors are delivered to the backstepping power controller, which eliminates steady state error. The output signals from backstepping power controller are used for switching signals generation by a five-level space vector modulator [13].

3.1. PCC virtual flux estimator

The principle of VF is based on assumption that the voltages imposed by the line power in combination with the AC side inductors can be considered as quantities related to a virtual AC motor, where R_F and L_F represent the stator resistance and leakage inductance of the virtual motor [17]. With the definitions:

$$\bar{\psi}_{PCC} = \int \bar{v} dt \tag{14}$$

In general R_F can be neglected and the voltage v can be expressed as in stationary α-β coordinates as follows:

$$\begin{aligned} v_\alpha &= u_{F\alpha} - L_F \frac{di_{F\alpha}}{dt} \\ v_\beta &= u_{F\beta} - L_F \frac{di_{F\beta}}{dt} \end{aligned} \tag{15}$$

The integrated of both sides of (15) gives:

$$\begin{aligned} \psi_{PCC\alpha} &= \int u_{F\alpha} dt - L_F i_{F\alpha} \\ \psi_{PCC\beta} &= \int u_{F\beta} dt - L_F i_{F\beta} \end{aligned} \tag{16}$$

The measured line currents $i_{F\alpha}$, $i_{F\beta}$ and the estimated virtual flux components $\psi_{PCC\alpha}$, $\psi_{PCC\beta}$ are used for SAPF power estimation.

3.2. Active and reactive powers estimator

Using the measured current and the estimated PCC virtual flux, the estimated active and reactive powers can be described by the following formulas [17]:

a) Active filter powers are:

$$\begin{aligned} p_F &= \omega(\psi_{PCC\alpha} i_{F\beta} - \psi_{PCC\beta} i_{F\alpha}) \\ q_F &= \omega(\psi_{PCC\alpha} i_{F\alpha} + \psi_{PCC\beta} i_{F\beta}) \end{aligned} \tag{17}$$

b) Nonlinear load powers are:

$$\begin{aligned} p_L &= \omega(\psi_{PCC\alpha} i_{L\beta} - \psi_{PCC\beta} i_{L\alpha}) \\ q_L &= \omega(\psi_{PCC\alpha} i_{L\alpha} + \psi_{PCC\beta} i_{L\beta}) \end{aligned} \tag{18}$$

Where: ω is the angular frequency.

Both power estimation equations are simple to calculate and do not require the computation of the current derivatives.

3.3. Active and reactive power model based on virtual flux

The backstepping power controller is based on instantaneous power time derivative behavior. From Equation (17), the derivatives of active and reactive powers are given by:

$$\begin{aligned} \frac{dp_F}{dt} &= \omega\left(\frac{d\psi_{PCC\alpha}}{dt} i_{F\beta} + \psi_{PCC\alpha} \frac{di_{F\beta}}{dt} - \frac{d\psi_{PCC\beta}}{dt} i_{F\alpha} - \psi_{PCC\beta} \frac{di_{F\alpha}}{dt} \right) \\ \frac{dq_F}{dt} &= \omega\left(\frac{d\psi_{PCC\alpha}}{dt} i_{F\alpha} + \psi_{PCC\alpha} \frac{di_{F\alpha}}{dt} + \frac{d\psi_{PCC\beta}}{dt} i_{F\beta} + \psi_{PCC\beta} \frac{di_{F\beta}}{dt} \right) \end{aligned} \tag{19}$$

For three-phase balanced system, the following relations can be written:

$$\begin{aligned} \psi_{PCC\alpha} &= \frac{v_\beta}{\omega}, \qquad \frac{d\psi_{PCC\alpha}}{dt} = -\omega\psi_{PCC\beta} \\ \psi_{PCC\beta} &= -\frac{v_\alpha}{\omega}, \qquad \frac{d\psi_{PCC\beta}}{dt} = \omega\psi_{PCC\alpha} \end{aligned} \tag{20}$$

Replacing (7), (20) into (19), power derivatives can be expressed as:

$$\begin{aligned} \frac{dp_F}{dt} &= -\omega q_F + \frac{\omega\psi_{PRC\alpha}}{L_F}\left(-R_F i_{F\beta} - \omega\psi_{PRC\alpha} + u_{F\beta}\right) \\ &\quad - \frac{\omega\psi_{PRC\beta}}{L_F}\left(-R_F i_{F\alpha} + \omega\psi_{PRC\beta} + u_{F\alpha}\right) \\ \frac{dq_F}{dt} &= \omega p_F + \frac{\omega\psi_{PRC\alpha}}{L_F}\left(-R_F i_{F\alpha} + \omega\psi_{PRC\beta} + u_{F\alpha}\right) \\ &\quad + \frac{\omega\psi_{PRC\beta}}{L_F}\left(-R_F i_{F\beta} - \omega\psi_{PRC\alpha} + u_{F\beta}\right) \end{aligned} \tag{21}$$

3.4. Backstepping controllers design

Backstepping is a systematic and recursive design methodology for nonlinear feedback control. This approach has emerged as powerful tools for stabilizing nonlinear systems both for tracking and regulation purposes [18]. The backstepping algorithm takes advantage of the idea that certain variables can be used as virtual controls to make the original high order system simple, thus the final control outputs can be derived step by step through suitable Lyapunov functions ensuring global stability. This control method has been successfully applied on a growing collection of plant. However, few papers are devoted to the backstepping control of power electronics converters [19]-[20]. In the following, the backstepping design procedure is applied to five-level shunt active power filter. As chosen in Figure 2, the control strategy is based on a cascade structure, namely, the output of outer voltage loop is used as reference signal in the inner power loop.

The approach adopted herein designs by breaking down a complex nonlinear system into smaller sub-systems, then designing control Lyapunov functions and virtual controls for these sub-systems. In order to design the control algorithm for active power filter with the aid of backstepping method, nonlinear differential Equation (12) and (21) must be portioned in three SISO subsystems at the following form:

$$\begin{aligned} \dot{\zeta}_k &= L_{f_k} h_k + L_{g_k} h_k u_k \\ y_k &= h_k(\xi_k); \ k = 1,2,3 \end{aligned} \tag{22}$$

Where ζ_k , u_k and y_k represent state, control input and output of k^{th} system, respectively. f_k and g_k are smooth fields, and h_k is a smooth scalar function. The term $L_{f_k} h_k$ stands for the Lie derivative of h_k with respect to f_k , similarly $L_{g_k} h_k$.

By identifying the first subsystem, based on equation (12), with (22), it can be yield:

$$\begin{aligned} &\zeta_1 = v_{dc}, \quad u_1 = p_F, \ \mathrm{y}_1 = h_1 = v_{dc}, \ L_{f_1} h_1 = 0 \\ &L_{g_1} h_1 = \frac{1}{C_{eq} v_{dc}} \end{aligned} \tag{23}$$

The second and the third subsystems are built based on the active and reactive derivative (21).

The identification of (21) with (22) leads to:

$$
\begin{aligned}
&\xi_2 = p_F \,,\; u_2 = \bar{u}_{F\alpha} = \frac{\omega}{L_F}\left(-\psi_{PCC\beta}u_{F\alpha} + \psi_{PCC\alpha}u_{F\beta}\right) \\
&y_2 = h_2 = p_F \,, L_{g_2}h_2 = 1 \\
&L_{f_2}h_2 = -\omega q_F + \frac{\omega}{L_F}\left[\psi_{PCC\alpha}\left(-R_F i_{F\beta} - \omega\psi_{PCC\alpha}\right) - \psi_{PCC\beta}\left(-R_F i_{F\alpha} + \omega\psi_{PCC\beta}\right)\right] \\
&\xi_3 = q_F \,,\; u_3 = \bar{u}_{F\beta} = \frac{\omega}{L_F}\left(\psi_{PCC\alpha}u_{F\alpha} + \psi_{PCC\beta}u_{F\beta}\right) \\
&y_3 = h_3 = q_F \,,\; L_{g_3}h_3 = 1 \\
&L_{f3}h_3 = \omega p_F + \frac{\omega}{L_F}\left[\psi_{PCC\alpha}\left(-R_F i_{F\alpha} + \omega\psi_{PCC\beta}\right) + \psi_{PCC\beta}\left(-R_F i_{F\beta} - \omega\psi_{PCC\alpha}\right)\right]
\end{aligned}
\tag{24}
$$

In following sections the backstepping method will be used for developing the *dc* voltage and power controllers.

3.4.1. DC Voltage Controller Synthesis

In order to ensure that the SAPF operates effectively it is important to maintain the *dc* capacitor voltage at a constant desired value. The backstepping *dc* voltage controller sets the active power of the inverter to regulate the *dc* voltage based on its reference value covering the inverter losses.

The purpose of this control is to achieve the dc voltage reference, so the first tracking error is defined as:

$$z_1 = y_1 - y_{1d} \tag{25}$$

Where:

$$y_{1d} = v_{dcref}$$

Differentiating (25) with respect to time, it is obtained that:

$$\dot{z}_1 = L_{f_1}h_1 + L_{g_1}h_1 p_{Fref} - \dot{y}_{1d} \tag{26}$$

The candidate function of Lyapunov is chosen as:

$$V_1 = \frac{1}{2}z_1^2 \tag{27}$$

The derivative of the Lyapunov function is expressed as:

$$\dot{V}_1 = z_1\dot{z}_1 = z_1(L_{f_1}h_1 + L_{g_1}h_1 p_{Fref} - \dot{y}_{1d}) \tag{28}$$

To guarantee the Lyapunov stability, the control law is chosen as:

$$p_{Fref} = \frac{-k_1 z_1 - L_{f_1}h_1 + \dot{y}_{1d}}{L_{g_1}h_1} \tag{29}$$

Where, k_1 is a positive constant.

3.4.2. Power Controller Synthesis

Using the backstepping approach, one can synthesize the control law forcing the active and reactive powers to follow the desired powers.

For the first step the following tracking-errors are considered:

$$\begin{aligned} z_2 &= y_2 - y_{2d} \\ z_3 &= y_3 - y_{3d} \end{aligned} \tag{30}$$

Where:

$$\begin{aligned} y_{2d} &= p_{Fref\_total} \\ y_{3d} &= q_{Fref\_total} \end{aligned}$$

Where:

$$\begin{aligned} p_{Fref\_total} &= p_{Fref} - \tilde{p}_L \\ q_{Fref\_total} &= q_{Fref} \end{aligned} \tag{31}$$

The resulting error dynamics equation can be expressed as:

$$\begin{aligned} \dot{z}_2 &= L_{f_2} h_2 + L_{g_2} h_2 \overline{u}_{F\alpha ref} - \dot{y}_{2d} \\ \dot{z}_3 &= L_{f_3} h_3 + L_{g_3} h_3 \overline{u}_{F\beta ref} - \dot{y}_{3d} \end{aligned} \tag{32}$$

The chosen Lyapunov functions are given by the following expressions:

$$\begin{aligned} V_2 &= \frac{1}{2} z_2^2 \\ V_3 &= \frac{1}{2} z_3^2 \end{aligned} \tag{33}$$

The time derivatives of Lyapunov functions V_2 and V_3 are given by:

$$\begin{aligned} \dot{V}_2 &= z_2 \dot{z}_2 = z_2 (L_{f_2} h_2 + L_{g_2} h_2 \overline{u}_{F\alpha ref} - \dot{y}_{2d}) \\ \dot{V}_3 &= z_3 \dot{z}_3 = z_3 (L_{f_3} h_3 + L_{g_3} h_3 \overline{u}_{F\beta ref} - \dot{y}_{3d}) \end{aligned} \tag{34}$$

In order to make negative the derivatives of Lyapunov functions, the intermediate control laws $\overline{u}_{F\alpha ref}$ and $\overline{u}_{F\beta ref}$ are proposed in the following equation:

$$\begin{aligned} \overline{u}_{F\alpha ref} &= \frac{-k_2 z_2 - L_{f_2} h_2 + \dot{y}_{2d}}{L_{g_2} h_2} \\ \overline{u}_{F\beta ref} &= \frac{-k_3 z_3 - L_{f_3} h_3 + \dot{y}_{3d}}{L_{g_3} h_3} \end{aligned} \tag{35}$$

Where, k_2 and k_3 are positive constants.

The relation between the intermediate and final control laws is given by:

$$\begin{bmatrix} \overline{u}_{F\alpha ref} \\ \overline{u}_{F\beta ref} \end{bmatrix} = D \begin{bmatrix} u_{F\alpha ref} \\ u_{F\beta ref} \end{bmatrix} \tag{36}$$

Where:

$$D = \frac{\omega}{L_F} \begin{bmatrix} -\psi_{PRC\beta} & \psi_{PRC\alpha} \\ \psi_{PRC\alpha} & \psi_{PRC\beta} \end{bmatrix}$$

The D matrix determinant is different to zero, so the final control laws are given as:

$$\begin{bmatrix} u_{F\alpha ref} \\ u_{F\beta ref} \end{bmatrix} = D^{-1} \begin{bmatrix} \overline{u}_{F\alpha ref} \\ \overline{u}_{F\beta ref} \end{bmatrix} \tag{37}$$

3.5. Space Vector Modulation with DC-Capacitor Voltages Balancing Strategy

In the five-level NPC topology, the voltages of the four series-connected dc-link capacitors must be confined to $v_{dc}/4$ to take advantage of the inverter. The dc-voltage backstepping control regulates only the total dc voltage. For this reason, the dc-capacitor voltages are kept equals using five-level SVPWM that takes advantages of redundant switching states to counteract the *dc* voltages drift phenomenon [21].

The five-level SVPWM technique can approximate the reference voltage vector, computed by backstepping power controller, using the nearest three vectors. They are selected to minimize the energy of the dc-capacitor voltages [21].

Figure 3 represents the space vector states for the five-level inverter there are 125 switching-state vectors. Applying Clark's transformation to all combinations of output voltages associated with the 125 switching-state vectors results in 60 nonzero voltage space vectors.

Projection of the vectors on $\alpha\beta$ coordinates forms a four-layer hexagon centered at the origin of the $\alpha\beta$ plane (Figure 3), and zero-voltage vectors are located at the origin of the plane.

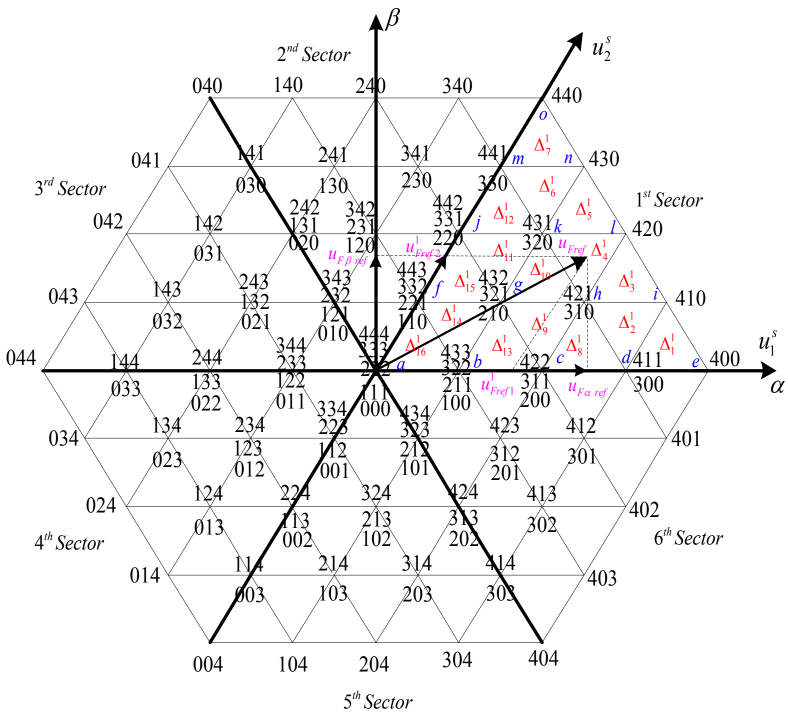

Figure 3. Space voltage vectors for a five-level inverter

3.5.1. Determination of the Space Vector Location

The space vector location is determined in two steps. The first step determines the sector number of where the vector lies. The second step determines the triangle in which the vector lies [22].

Step 1: Sector number computation.

The reference voltage vector magnitude and its angle are determined from:

$$u_{Fref} = \sqrt{u_{F\alpha ref}^2 + u_{F\beta ref}^2} \quad \text{and} \quad \theta = \tan 2^{-1}\left(\frac{u_{F\beta ref}}{u_{F\alpha ref}}\right) \tag{38}$$

Where, the tan 2^{-1} function returns the four-quadrant inverse tangent. Once the value of θ is calculated, the sector numbers are given by [22]:

$$S = \text{ceil}\left(\frac{\theta}{\pi/3}\right) \in \{1,2,3,4,5,6\} \tag{39}$$

Where *ceil* is the C-function that adjusts any real number to the nearest, but higher, integer.

Step 2: Triangle identification.

Reference vector u_{Fref} is projected on the axes of 60° coordinate system [21]. In each sector *S*, the normalized projected components are $u^s_{Fref\,1}$ and $u^s_{Fref\,2}$ given by (40). Fig. 3 shows the projection of u_{Fref} in the first sector.

$$\begin{aligned} u^S_{Fref1} &= \frac{u_{Fref}\cos(\theta-(S-1)\frac{\pi}{3}))-\frac{u_{Fref}}{\sqrt{3}}\sin(\theta-(S-1)\frac{\pi}{3})}{\sqrt{\frac{2}{3}}\frac{v_{dc}}{2}} \\ u^S_{Fref2} &= \frac{\frac{2}{\sqrt{3}}u_{Fref}\sin(\theta-(S-1)\frac{\pi}{3})}{\sqrt{\frac{2}{3}}\frac{v_{dc}}{2}} \end{aligned} \tag{40}$$

In order to identify the triangle where the required reference is located, the following integers are used:

$$\begin{aligned} l^S_1 &= \text{int}\left(u^S_{Fref1}\right) \\ l^S_2 &= \text{int}\left(u^S_{Fref2}\right) \end{aligned} \tag{41}$$

Where the *int*() function returns the nearest integer that is less than or equal to its argument. The triangle number is obtained according to the value of l^S_1 and l^S_2, as shown in Table 2:

Table 2. Triangle identification in each sector *S*

l^S_1	l^S_2	Δ^S_i $(i \in \{1,\ldots,16\})$
0	0	Δ^S_{16} Si $(u^S_{ref1}+u^S_{ref2}<1)$ Δ^S_{14} Si $(u^S_{ref1}+u^S_{ref2}\geq 1)$
1	0	Δ^S_{13} Si $(u^S_{ref1}+u^S_{ref2}<2)$ Δ^S_{9} Si $(u^S_{ref1}+u^S_{ref2}\geq 2)$
2	0	Δ^S_{8} Si $(u^S_{ref1}+u^S_{ref2}<3)$ Δ^S_{2} Si $(u^S_{ref1}+u^S_{ref2}\geq 3)$
3	0	Δ^S_1
0	1	Δ^S_{15} Si $(u^S_{ref1}+u^S_{ref2}<2)$ Δ^S_{11} Si $(u^S_{ref1}+u^S_{ref2}\geq 2)$
1	1	Δ^S_{10} Si $(u^S_{ref1}+u^S_{ref2}<3)$ Δ^S_{4} Si $(u^S_{ref1}+u^S_{ref2}\geq 3)$
2	1	Δ^S_3
0	2	Δ^S_{12} Si $(u^S_{ref1}+u^S_{ref2}<3)$ Δ^S_{6} Si $(u^S_{ref1}+u^S_{ref2}\geq 3)$
1	2	Δ^S_5
0	3	Δ^S_7

3.5.2. Duration Time Calculation

On-duration time intervals of the switching voltage vectors adjacent to the reference voltage vector u_{Fref} of a five-level NPC are calculated as follows:

$$\begin{aligned} &u_x^{\Delta_i^s} t_x^{\Delta_i^s} + u_y^{\Delta_i^s} t_y^{\Delta_i^s} + u_z^{\Delta_i^s} t_z^{\Delta_i^s} = u_{Fref} T_s \\ &t_x^{\Delta_i^s} + t_y^{\Delta_i^s} + t_z^{\Delta_i^s} = T_s \end{aligned} \tag{42}$$

Where T_s is the switching period, $u_x^{\Delta_i^s}$, $u_y^{\Delta_i^s}$ and $u_z^{\Delta_i^s}$ are the three switching vectors adjacent to the reference voltage vector located in the triangle $\Delta_i^s (i = 1,...,16)$ formed by the vertices (x,y,z) and $t_x^{\Delta_i^s}$, $t_y^{\Delta_i^s}$ and $t_z^{\Delta_i^s}$ are the calculated on-duration time intervals of the switching vectors, respectively.

Expression (42) can by decomposed in the 60° coordinates system as follows:

$$\begin{aligned} &u_{x1}^{\Delta_i^s} t_x^{\Delta_i^s} + u_{y1}^{\Delta_i^s} t_y^{\Delta_i^s} + u_{z1}^{\Delta_i^s} t_z^{\Delta_i^s} = u_{Fref1} T_s \\ &u_{x2}^{\Delta_i^s} t_x^{\Delta_i^s} + u_{y2}^{\Delta_i^s} t_y^{\Delta_i^s} + u_{z2}^{\Delta_i^s} t_z^{\Delta_i^s} = u_{Fref2} T_s \\ &t_x^{\Delta_i^s} + t_y^{\Delta_i^s} + t_z^{\Delta_i^s} = T_s \end{aligned} \tag{43}$$

The coordinates of all vertices of S^{th} sector are given in Table 3.

Table 3. Vertices coordinate in S^{th} sector

vertices	coordinates
A	$(u_{A1}^{\Delta_i^s}, u_{A2}^{\Delta_i^s}) = (0,0)$
B	$(u_{B1}^{\Delta_i^s}, u_{B2}^{\Delta_i^s}) = (1,0)$
C	$(u_{C1}^{\Delta_i^s}, u_{C2}^{\Delta_i^s}) = (2,0)$
D	$(u_{D1}^{\Delta_i^s}, u_{D2}^{\Delta_i^s}) = (3,0)$
E	$(u_{E1}^{\Delta_i^s}, u_{E2}^{\Delta_i^s}) = (4,0)$
F	$(u_{F1}^{\Delta_i^s}, u_{F2}^{\Delta_i^s}) = (0,1)$
G	$(u_{G1}^{\Delta_i^s}, u_{G2}^{\Delta_i^s}) = (1,1)$
H	$(u_{H1}^{\Delta_i^s}, u_{H2}^{\Delta_i^s}) = (2,1)$
I	$(u_{I1}^{\Delta_i^s}, u_{I2}^{\Delta_i^s}) = (3,1)$
J	$(u_{J1}^{\Delta_i^s}, u_{J2}^{\Delta_i^s}) = (0,2)$
K	$(u_{K1}^{\Delta_i^s}, u_{K2}^{\Delta_i^s}) = (1,2)$
L	$(u_{L1}^{\Delta_i^s}, u_{L2}^{\Delta_i^s}) = (2,2)$
M	$(u_{M1}^{\Delta_i^s}, u_{M2}^{\Delta_i^s}) = (0,3)$
N	$(u_{N1}^{\Delta_i^s}, u_{N2}^{\Delta_i^s}) = (1,3)$
O	$(u_{O1}^{\Delta_i^s}, u_{O2}^{\Delta_i^s}) = (0,4)$

Substituting the coordinates of u_x, u_y and u_z from Table 3 in (43), in each triangle, the on-duration time intervals are summarized in Table 4. These duration times are valid in all sectors.

The significant outcome of the proposed algorithm is its inherent simplicity. Unlike the conventional SVM algorithm that requires solution of several sets of trigonometric equations for calculation of on-duration time intervals. Therefore, the proposed SVM algorithm is much simpler and easier for digital implementation since it reduces the hardware and software complexity and decreases the required computational time.

Table 4. Duration time in each triangle of the S^{th} sector

Triangle	Duration time intervals $t_x^{\Delta_i^S}$	$t_y^{\Delta_i^S}$	$t_z^{\Delta_i^S}$
$\Delta_1^S(x,y,z)=(D,E,I)$	$T_s-t_y^{\Delta_i^S}-t_z^{\Delta_i^S}$	$\left(u_{ref1}^S-3\right)T_s$	$u_{ref2}^S T_s$
$\Delta_2^S(x,y,z)=(I,H,D)$	$T_s-t_y^{\Delta_i^S}-t_z^{\Delta_i^S}$	$\left(3-u_{ref1}^S\right)T_s$	$\left(1-u_{ref2}^S\right)T_s$
$\Delta_3^S(x,y,z)=(H,I,L)$	$T_s-t_y^{\Delta_i^S}-t_z^{\Delta_i^S}$	$\left(u_{ref1}^S-2\right)T_s$	$\left(u_{ref2}^S-1\right)T_s$
$\Delta_4^S(x,y,z)=(L,K,H)$	$T_s-t_y^{\Delta_i^S}-t_z^{\Delta_i^S}$	$\left(2-u_{ref1}^S\right)T_s$	$\left(2-u_{ref2}^S\right)T_s$
$\Delta_5^S(x,y,z)=(K,L,N)$	$T_s-t_y^{\Delta_i^S}-t_z^{\Delta_i^S}$	$\left(u_{ref1}^S-1\right)T_s$	$\left(u_{ref2}^S-2\right)T_s$
$\Delta_6^S(x,y,z)=(N,M,K)$	$T_s-t_y^{\Delta_i^S}-t_z^{\Delta_i^S}$	$\left(1-u_{ref1}^S\right)T_s$	$\left(3-u_{ref2}^S\right)T_s$
$\Delta_7^S(x,y,z)=(M,N,O)$	$T_s-t_y^{\Delta_i^S}-t_z^{\Delta_i^S}$	$u_{ref1}^S T_s$	$\left(u_{ref2}^S-3\right)T_s$
$\Delta_8^S(x,y,z)=(C,D,H)$	$T_s-t_y^{\Delta_i^S}-t_z^{\Delta_i^S}$	$\left(u_{ref1}^S-2\right)T_s$	$u_{ref2}^S T_s$
$\Delta_9^S(x,y,z)=(H,G,C)$	$T_s-t_y^{\Delta_i^S}-t_z^{\Delta_i^S}$	$\left(2-u_{ref1}^S\right)T_s$	$\left(1-u_{ref2}^S\right)T_s$
$\Delta_{10}^S(x,y,z)=(G,H,K)$	$T_s-t_y^{\Delta_i^S}-t_z^{\Delta_i^S}$	$\left(u_{ref1}^S-1\right)T_s$	$\left(u_{ref2}^S-1\right)T_s$
$\Delta_{11}^S(x,y,z)=(K,J,G)$	$T_s-t_y^{\Delta_i^S}-t_z^{\Delta_i^S}$	$\left(1-u_{ref1}^S\right)T_s$	$\left(2-u_{ref2}^S\right)T_s$
$\Delta_{12}^S(x,y,z)=(J,K,M)$	$T_s-t_y^{\Delta_i^S}-t_z^{\Delta_i^S}$	$u_{ref1}^S T_s$	$\left(u_{ref2}^S-2\right)T_s$
$\Delta_{13}^S(x,y,z)=(B,C,J)$	$T_s-t_y^{\Delta_i^S}-t_z^{\Delta_i^S}$	$\left(u_{ref1}^S-1\right)T_s$	$u_{ref2}^S T_s$
$\Delta_{14}^S(x,y,z)=(G,F,B)$	$T_s-t_y^{\Delta_i^S}-t_z^{\Delta_i^S}$	$\left(1-u_{ref1}^S\right)T_s$	$\left(1-u_{ref2}^S\right)T_s$
$\Delta_{15}^S(x,y,z)=(F,G,J)$	$T_s-t_y^{\Delta_i^S}-t_z^{\Delta_i^S}$	$u_{ref1}^S T_s$	$\left(u_{ref2}^S-1\right)T_s$
$\Delta_{16}^S(x,y,z)=(A,B,F)$	$T_s-t_y^{\Delta_i^S}-t_z^{\Delta_i^S}$	$u_{ref1}^S T_s$	$u_{ref2}^S T_s$

3.5.3. DC-capacitor Voltages Balancing Based on Minimum Energy Property

In a five-level NPC inverter, the total energy E of dc-link capacitors is:

$$E=\frac{1}{2}\sum_{j=1}^{4}C_j v_{C_j}^2 \tag{44}$$

When all capacitor voltages are balanced, the total energy E reaches its minimum of $E_{\min}=Cv_{dcref}^2/8$, with v_{dcref} is the desired value of dc voltage. This condition is called the minimum energy property which can be used as the basic principle for dc-capacitor voltages balancing and control [21]. The adopted control method should minimize a quadratic cost function J associated with voltage deviation of the dc-capacitors. The cost function is defined as follows:

$$J=\frac{1}{2}C\sum_{j=1}^{4}\left(v_{C_j}-\frac{v_{dc}}{4}\right)^2 \tag{45}$$

The mathematical condition to minimize J is:

$$\sum_{j=1}^{4}\Delta v_{C_j} i_{C_j} \le 0 \tag{46}$$

Where:

$$\Delta v_{Cj}=v_{Cj}-v_{dc}/2,\quad j=1,2,3,4$$

The capacitor currents are affected by the dc-side intermediate branch currents, i_1, i_2 and i_3. Thus, it is advantageous to express (46) in terms of i_1, i_2 and i_3. The dc-capacitor currents are expressed as:

$$i_{C_j} = \frac{1}{4}\sum_{x=1}^{3} x i_x^S - \sum_{x=j}^{3} i_x^S, \qquad j = 1,2,3,4. \tag{47}$$

By substituting (47) in (46), the condition to achieve voltage balancing is deduced as:

$$\sum_{j=1}^{4} \Delta v_{C_j} \left(\frac{1}{4}\sum_{x=1}^{3} x i_x^S - \sum_{x=j}^{3} i_x^S \right) \leq 0 \tag{48}$$

When the DC link voltages v_{Cj} are closed to their reference v_{dc} /4, the following condition is verified:

$$\sum_{j=1}^{4} \Delta v_{C_j} = 0 \tag{49}$$

Using (49), the Equation (48) can be written as:

$$\sum_{j=1}^{3} \Delta v_{C_j} \left(\sum_{x=j}^{3} i_x^S \right) \geq 0 \tag{50}$$

Applying the averaging operator, over one sampling period, to (50) results in:

$$\frac{1}{T_s}\int_{kT_s}^{(k+1)T_s} \left[\sum_{j=1}^{3} \Delta v_{C_j} \left(\sum_{x=j}^{3} i_x^S \right) \right] dt \geq 0 \tag{51}$$

Assuming that sampling period T_s, as compared to the time interval associate with the dynamics of capacitor voltages, is adequately small, the capacitor voltages can be assumed to remain constant over one sampling period [21] and, consequently, (51) is simplified to:

$$\sum_{j=1}^{3} \Delta v_{C_j}(k) \left(\sum_{x=j}^{3} \overline{i}_x^S(k) \right) \geq 0 \tag{52}$$

Where, $\Delta v_{Cj}(k)$ is the voltage drift at sampling period k, and $\overline{i_j}, j = 1,2,3$ is the averaged value of the i_j.

The current $\overline{i_j}$ should be computed for different combinations of adjacent redundant switching states over a sampling period and the best combination which maximizes (52) is selected.

4. SIMULATION RESULTS

The proposed backstepping controller for three-phase five-level SAPF has been simulated and compared with conventional PI controller. The parameters used are shown in Table 5.

Table 5. Basic parameters of the system under study

RMS value of phase voltage	*5.5 kV*
DC-link capacitor C	5 mF
Source impedance R_s, L_s	0.1 mΩ, 0.1 mH
Filter impedance R_F, L_F	0.1 mΩ, 1 mH
Switching frequency f_s	4 kHz
Fundamental frequency f	50 Hz
DC-link voltage reference $v_{dc\,ref}$	20 kV
Diode rectifier load R_l, L_l	200 Ω, 1mH
Input diode rectifier impedance R_L, L_L	100 mΩ, 1 mH
Sampling frequency	1 MHz
k_1, k_2, k_3 constants	70, 2.10^5, 2.10^5

The goal of the simulation is to examine the capability of the controller to fulfill the following four different aspects.

a) Harmonic current compensation
b) Dynamic response performance
c) Parameters variation
d) Distorted grid phase voltage

4.1. Harmonic Current Compensation

The AC supply current of phase (a) and its harmonic spectrums before and after compensation are illustrated in Figure 4, 5 and 6. It results that the SAPF decreases the total harmonic distortion in the supply currents from 29.68% to 2.96% with PI control and to 1.47 % with backstepping control. So, the distortion in supply current with backstepping control is less than in case of PI control method.

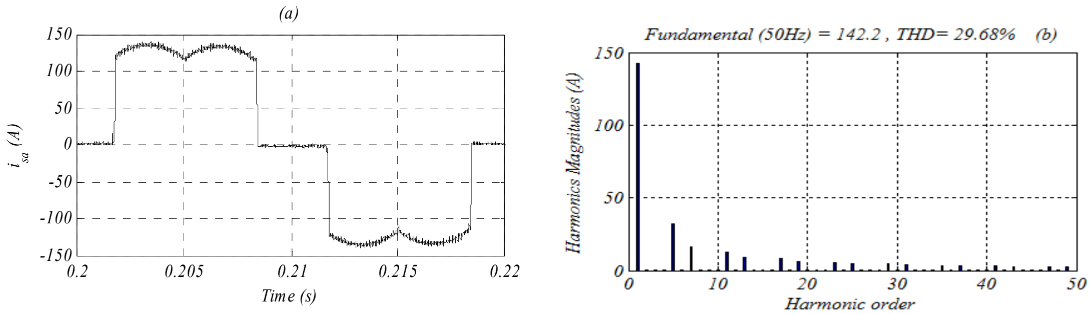

Figure 4. (a) Supply current before harmonics compensation, (b) Its harmonic spectrum

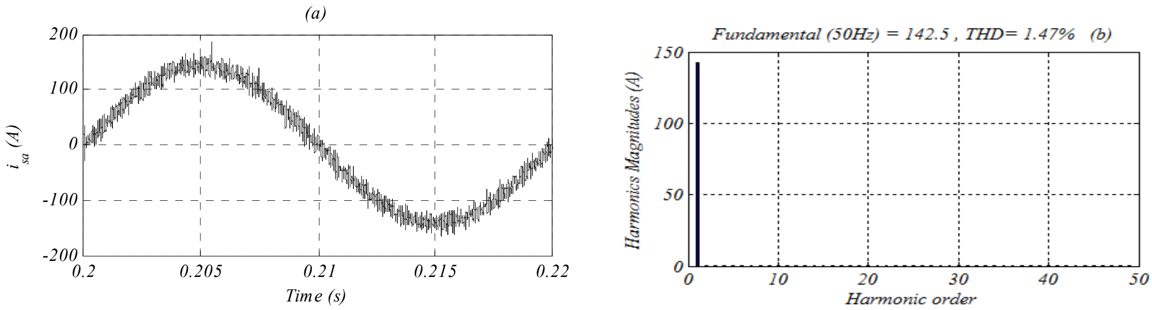

Figure 5. (a) Supply current after harmonics compensation using backstepping controller, (b) Its harmonic spectrum

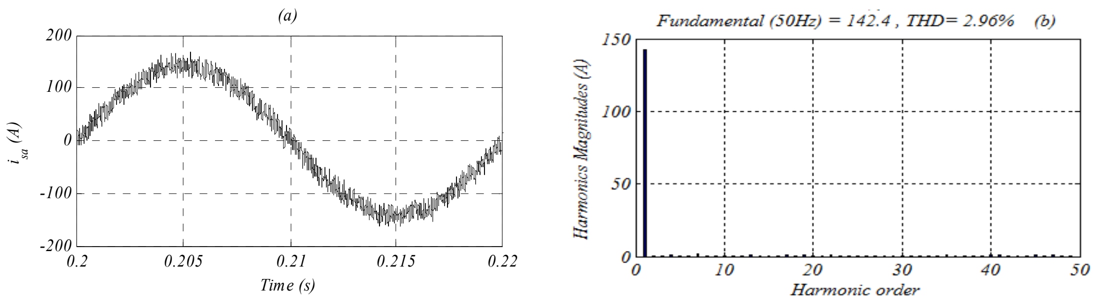

Figure 6. (a) Supply current after harmonics compensation using PI controller, (b) Its harmonic spectrum

4.2. Dynamic Response Performance

In this section, the performances of the backstepping and PI controllers are analyzed under 100% step charge in the resistance load at t = 0.5s.

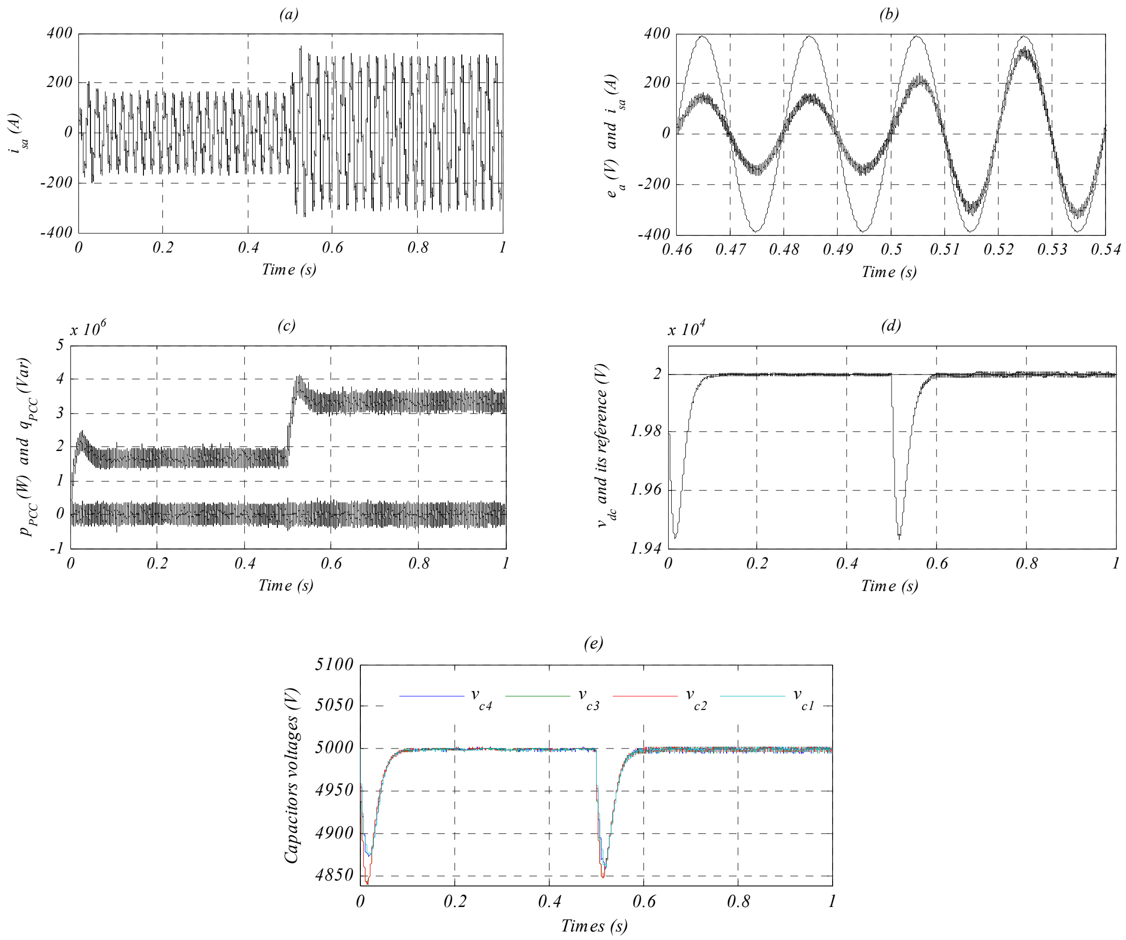

Figure 7. Simulation results of the proposed VFDPC-SVM using backstepping controller. (a) Source current. (b) Reduced source voltage and source current of a-phase (c) PCC active and reactive powers. (d) DC-link voltage v_{dc}. (e) DC capacitors voltages

The dynamic behavior under a step change of the load is presented in Figure 7 and 8 for backstepping and PI controllers respectively. The active power was changed stepwise from 1.7 to 3.4 MW. For clarity, a phase-a current is shown for illustration and the corresponding phase voltage is scaled down by a factor of 1/20. It can be observed that the unity power factor operation is successfully achieved, even in this transient state. As a result, the DC-bus voltage decreases, since the DC capacitors discharge. In a short time, the backstepping controller starts to respond due to the voltage error signal, which is the difference between the DC-bus reference voltage and the DC bus actual voltage. The output reference power of the controller will increase slowly to attain the required active power.

When, the instantaneous value of the active power drawn from the grid is equivalent to the active power consumed by the load, the DC-bus voltage stops decreasing and the inverter stops supplying the active power. Afterwards, the DC-bus voltage returns to the value according to the DC-bus reference voltage (without overshoot with backstepping control). When the DC-bus voltage is at its reference value, the new steady state has been achieved with new grid current amplitude.

From Figure 7(e), it is important to note that the application of the proposed redundant vectors based five-level SVM control maintains these voltages constant around the reference of 5kV.

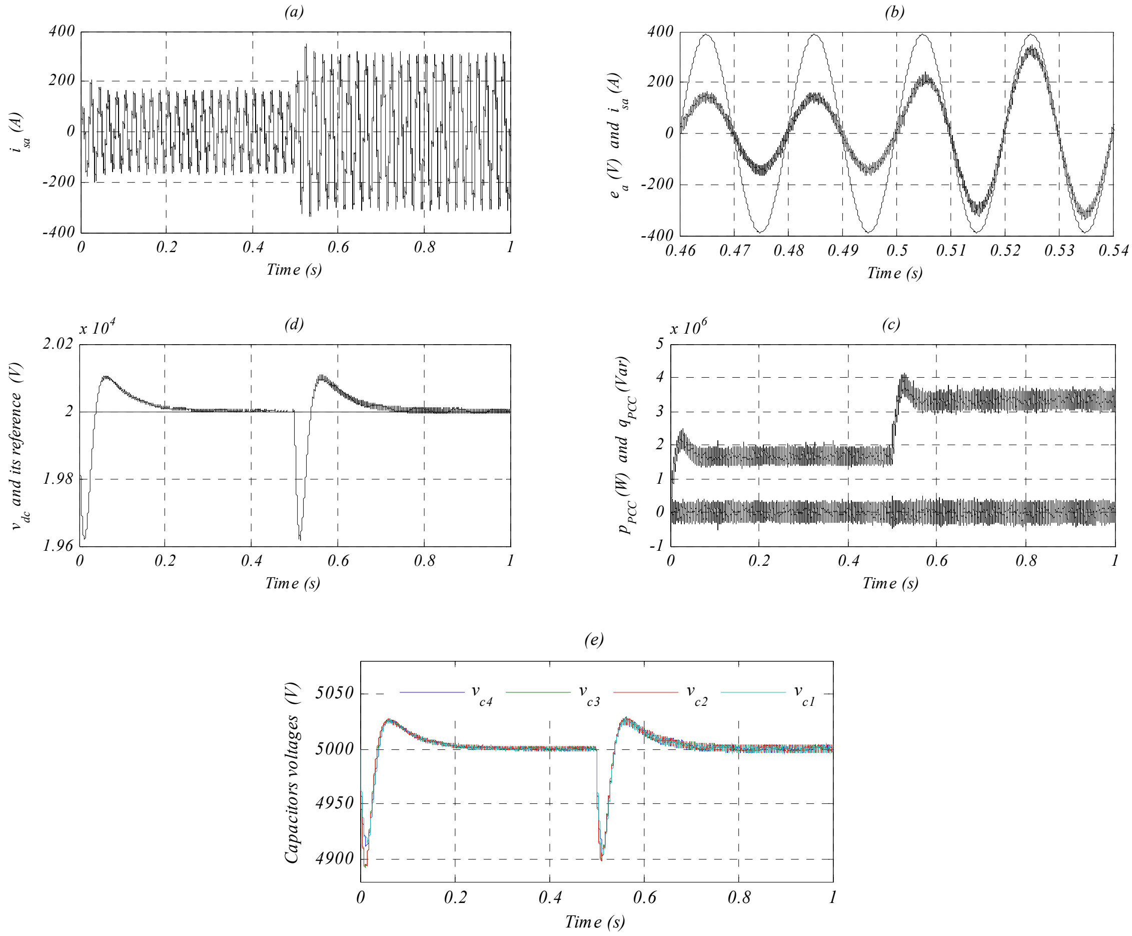

Figure 8. Simulation results of conventional VFDPC-SVM using PI controller. (a) Source current. (b) Reduced source voltage and source current of a-phase (c) PCC active and reactive powers. (d) DC-link voltage v_{dc}. (e) DC capacitors voltages

3.3. Parameters Variation

The values of the inverter-side inductors L_F may vary according to the operation point and aging. A small variation in this parameter may cause erroneous virtual-flux estimation, and consequently, an incorrect amount of active and reactive powers is generated by the inverter. To show the influence of these variations in system accuracy, simulations with different inductor values are analyzed, Figure 9(a).

The switching frequency is also a biasing factor on the harmonic quality of the line current as well as the size of SAPF inductances [23-24]. It is important to show its influence on the line current THD, Figure 9(b)

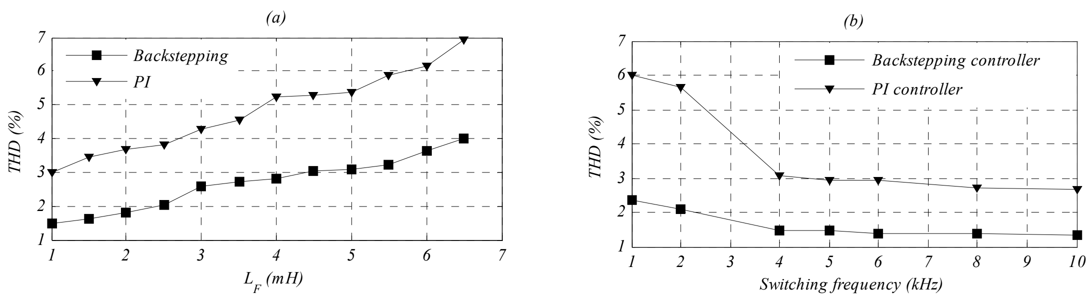

Figure 9. Simulation results of robustness examination. (a) THD of line current versus value of SAPF inductor (b) THD of line current versus value of switching frequency.

Figure 9(a) shows that the THD increases with the increase of the coupling inductance L_F. The proposed VFDPC-SVM using backstepping controller gives the best results for all values of L_F. However, for conventional VFDPC-SVM, the increase of L_F leads immediately to the increase in current THD.

From the Figure 9(b) one notices well that the THD decreases remarkably with increase of the switching frequency. It can be concluded that the VFDPC-SVM based on backstepping controller can be operated with reduced switching frequency (1 kHz).

3.4. Distorted Grid Phase Voltage

In an ideal situation, the grid usually consists of a balanced three-phase power system with sinusoidal line voltage-waves. However, the line voltage is frequently distorted and the systems which are connected to the grid should be able to tolerate this situation. One of the main disturbances is the presence of line voltage harmonics of order 5, 7 and 11. Figure 10 shows the waveforms in which a fifth harmonic voltage component of 10% is intentionally superimposed on the fundamental grid voltage.

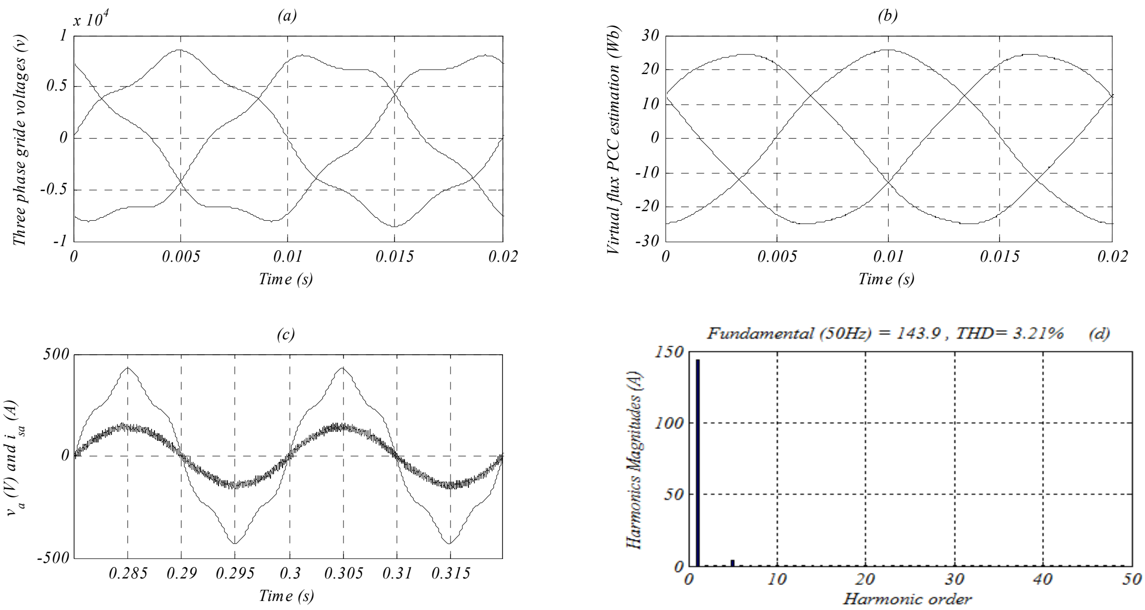

Figure 10. Simulation results of proposed backstepping VFDPC-SVM control with distorted grid phase voltage. (a) Three-phase grid voltages. (b) PCC virtual flux. (c) Reduce source voltage and source current of a-phase. (d) Harmonic spectrum of line current.

It can be observed that the grid current is nearly sinusoidal shape (THD = 3.21%) and unity power factor operation is successfully achieved even in existence of the distorted grid voltages as shown in Figure 10. This result is due to fact that voltage was replaced by virtual flux (the integrator behaves like a low-pass filter).

5. CONCLUSION

This paper has investigated a virtual flux direct power control based on backstepping approach for three-phase shunt active power filter using a five-level inverter. The proposed control scheme is intended to achieve harmonics elimination, reactive power compensation, and *dc* voltage regulation. Simulation results show that the backstepping-based control strategy significantly reduces the current distortion to values allowed by international standards, and regulates the power factor observed in the common coupling point between the nonlinear load and the power distribution system as well as exhibits excellent transient response during large load variations. When compared to the conventional control, the backstepping control offers substantial improvements on harmonic content of supply current, and robustness to the filter parameters variations. These results confirm that the backstepping control strategy provides higher performance than the traditional control. Thus, the proposed method can be useful to different applications such as motor drives, wind generators and power supply networks interconnection.

REFERENCES

[1] H Akagi. Modern Active Filters and Traditional Passive Filters. *Bulletin of the Polish Academy of Sciences Technical Sciences*. 2006; 54(3): 255-269.
[2] I Habi, et al. *Using the Shunt Active Power Filter for Compensation of the Distorted and Unbalanced Power System Voltage.* Proceedings of World Academy of Science, Engineering and Technology. 2006; 17: 287-291.
[3] AA Valdez, et al. An Adaptive Controller for the Shunt Active Filter Considering a Dynamic Load and the Line Impedance. *IEEE Transaction on Control Systems Technology*. 2009; 17(2): 458- 464.
[4] I Colak, E Kabalci, R Bay. Review of Multilevel Voltage Source Inverter Topologies and Control Schemes. *Energy Conversion and Management*. 2010; 52: 1114–1128.
[5] E Babaei, et al. Reduction of DC Voltage Sources and Switches in Asymmetrical Multilevel Converters Using a Novel Topology. *Electric Power Systems Research*. 2007; 77: 1073–1085.
[6] NF Mailah, et al. Neutral-Point-Clamped Multilevel Inverter Using Space Vector Modulation. *European Journal of Scientific Research*. 2009; 28(1): 82-91.
[7] S Barkati, et al. Harmonic Elimination in Diode-Clamped Multilevel Inverter Using Evolutionary Algorithms. *Electric Power Systems Research*. 2008; 78: 1736-1746.
[8] ME Ortúzar, et al. Voltage-Source Active Power Filter Based on Multilevel Converter and Ultra capacitor DC Link. *IEEE Transaction on Industrial Power Electronics*. 2006; 53(3): 477-485.
[9] S Saad, et al. Fuzzy Logic Controller for Three-Level Shunt Active Filter Compensating Harmonics and Reactive Power. *Electric Power Systems Research*. 2009; 79: 1337–1341.
[10] A Munduate, et al. Robust Model-Following Control of a Three-Level Neutral Point Clamped Shunt Active Filter in the Medium Voltage Range. *Electrical Power and Energy Systems*. 2009; 31: 577-588.
[11] G Zhou, et al. Direct Power Control of a Multilevel Inverter Based Active Power Filter. *Electric Power Systems Research*. 2007; 77: 284–294.
[12] N Belhaouchet, et al. A Novel Adaptive HBCC Technique for Three-phase Shunt APF. *Electric Power Systems Research*. 2009; 79: 1097–1104.
[13] M Cichowlas, et al. Active Filtering Function of Three-Phase PWM Boost Rectifier Under Different Line Voltage Conditions. *IEEE Transaction on Industrial Power Electronics*. 2005; 52(2): 410-419.
[14] A Chaoui, et al. DPC Controlled Three-Phase Active Filter for Power Quality Improvement. *Electrical Power and Energy Systems*. 2008; 30: 476–485.
[15] M Malinowski, et al. Simple Direct Power Control of Three-Phase PWM Rectifier Using Space-Vector Modulation (DPC-SVM). *IEEE Transaction on Industrial Power Electronics*. 2004; 51(2): 447-454.
[16] BS Chen, et al. Direct Power Control of Active Filters with Averaged Switching Frequency Regulation. *IEEE Transaction on. Power Electronics*. 2008; 23(6): 2729-2737.
[17] M Malinowski, et al. Virtual Flux Based Direct Power Control of Three-Phase PWM Rectifiers. *IEEE Transaction on Industry Applications*. 2001; 37(4): 1019-1027.
[18] BR Lin, et al. Implementation of a three phase capacitor clamped active power filter under unbalanced condition. *IEEE Transaction on Industrial Electronics*. 2006; 53(5): 1621-1630.
[19] G Zhou, et al. Direct power control of a multilevel inverter based active power filter. *Electric Power Systems Research*. 2007; 77: 284-294.
[20] O Vodyakho, et al. Novel direct current space-vector control for shunt active power filters based on the three-level inverter. *IEEE Transaction on Industrial Power Electronics*. 2008; 23(4): 1668-1678.
[21] M Saeedifard, et al. Analysis and Control of DC-Capacitor-Voltage-Drift Phenomenon of a Passive Front-End Five-Level Converter. *IEEE Transaction on Industrial Electronics*. 2007; 54(6): 3255-3266.
[22] HA Hotait, et al. Capacitor Voltage Balancing Using Redundant States of Space Vector Modulation for Five-Level Diode Clamped Inverters. *IET Power Electronics*. 2010; 3(2): 292-313.
[23] X Zhenfeng, et al. A Shunt Active Power Filter with Enhanced Dynamic performance using DualRepetitive Controller and Predictive Compensation. *International Journal of Power Electronics and Drive Systems (IJPEDS).* 2013; 3(2): 209-217.
[24] C Zhang, et al. Shunt Active Power Filter System Design for Interharmonic. *International Journal of Power Electronics and Drive Systems (IJPEDS)*. 2013; 3(4): 373-383.